7

Heteronuclear NMR Studies of the Molecular Dynamics of Staphylococcal Nuclease

Dennis A. Torchia, Linda K. Nicholson, Holly B. R. Cole and Lewis E. Kay

1 Introduction

During the past decade tremendous progress has been made in developing NMR techniques to determine the structure of proteins in solution. For proteins containing less than *c.* 100 residues, essentially complete proton signal assignments can be obtained using two- and three-dimensional homonuclear (proton) pulse sequences (Wüthrich, 1986; Clore and Gronenborn, 1989). These assignments together with distance and dihedral angle constraints, derived from NOEs and coupling constants, respectively, provide sufficient information to determine the three-dimensional structure of the protein. Recently it has been shown that NMR methods can be applied to larger proteins, containing up to *c.* 200 residues, by combining heteronuclear labelling (with ^{13}C and/or ^{15}N) with sophisticated double- and triple-resonance multidimensional techniques (Bax *et al.*, 1990; Fesik *et al.*, 1990; Ikura *et al.*, 1990; Kay *et al.*, 1990a,b; Clore *et al.*, 1991a,b; Pelton *et al.*, 1991).

Because of the great interest in and importance of protein structure–function relationships, most NMR studies have been directed towards structure elucidation. However, it is widely recognized that proteins undergo significant internal motions on a wide range of time-scales (Karplus and McCammon, 1986). It will be necessary to delineate these motions in order to determine the range of structures available to proteins. In addition, protein dynamics have important functional roles in protein folding, enzyme action and molecular recognition. At a more fundamental level, measurement of quantities related to the rates and

amplitudes of internal motions in proteins will provide data that can test the predictions of molecular dynamics calculations. The comparison of theory with experiment will result in improved potential functions that will enhance our understanding of the fundamental interactions between atoms in proteins.

While proton–proton NOEs and *J* couplings provide most of the information about protein structure, heteronuclear, rather than proton, relaxation data are better suited to yield information about motions of specific internuclear vectors in proteins. Although pioneering studies of natural abundance ^{13}C relaxation in proteins were carried out over ten years ago (Wittebort *et al.*, 1979; Richarz *et al.*, 1980; London, 1989), these studies were limited by lack of sequential assignments, and the low sensitivity and resolution afforded by one-dimensional ^{13}C spectra. Modern two-dimensional NMR experiments, in which heteronuclear relaxation is measured by proton detection, yield spectra having high sensitivity and resolution (Kay *et al.*, 1989; Nirmala and Wagner, 1989). In addition, double- and triple-resonance multidimensional NMR experiments provide essentially complete heteronuclear signal assignments (Clore *et al.*, 1990a; Ikura *et al.*, 1991; Pelton *et al.*, 1991).

Here we focus upon the application of these new NMR approaches to the study of the internal dynamics of recombinant staphylococcal nuclease, SNase, an enzyme containing 149 amino acid residues (Shortle, 1983). We begin with a brief summary of equations that relate the measured spin relaxation parameters to the model-free parameters (S, τ_m and τ_e) of Lipari and Szabo (1982a,b). We then discuss (a) the pulse sequences that are used to measure the relaxation parameters and (b) the method of determining the uncertainties in the relaxation parameters and the associated model-free parameters. Next we discuss how one derives information about molecular motion from the model-free parameters. We then review the application of heteronuclear relaxation measurements to study internal dynamics of SNase in solution and, for the purpose of comparison, in the crystalline state. We conclude with a discussion of the prospects for future NMR studies of protein dynamics.

2 Relaxation Theory

Nuclear Spin Relaxation

It has been recognized from the inception of the NMR technique (Bloembergen *et al.*, 1948) that nuclear spin relaxation rates are closely related to molecular motions. In the case of a spin $I = \frac{1}{2}$ heteronucleus (designated A) such as ^{13}C or ^{15}N, the three commonly measured relaxation parameters are the longitudinal relaxation time, T_1, the

transverse relaxation time, T_2 and the A-{^{1}H} nuclear Overhauser enhancement (NOE) (Abragam, 1961). When the heteronucleus, A, is bonded to a single proton, X, the dominant relaxation mechanism is the AX dipolar interaction, while chemical shift anisotropy is a secondary but significant relaxation mechanism, particularly as field strength increases. Provided that the dipolar and CSA relaxation mechanisms are uncorrelated, the expressions for the relaxation parameters of a spin A bonded to a single proton are given by (Kay *et al.*, 1989)

$$1/T_1 = d^2[J(\omega_A - \omega_X) + 3J(\omega_A) + 6J(\omega_A + \omega_X)] + c^2J(\omega_A) \quad (7.1)$$

$$1/T_2 = 0.5d^2[4J(0) + J(\omega_A - \omega_X) + 3J(\omega_A) + 6J(\omega_X) + 6J(\omega_A + \omega_X)] + (1/6)c^2[4J(0) + 3J(\omega_A)] \quad (7.2)$$

$$\text{NOE} = 1 + \{(\gamma_X/\gamma_A)d^2[6J(\omega_A + \omega_X) - J(\omega_A - \omega_X)]T_1\} \quad (7.3)$$

In these Equations $d^2 = 0.1[\gamma_A\gamma_X h/(2\pi \langle 1/r_{AX}^3\rangle)]^2$ and $c^2 = (2/15)[\gamma_A B_0 (\sigma_\parallel - \sigma_\perp)]^2$, γ_i is the gyromagnetic ratio of spin i, h is Planck's constant, r_{AX} is the AX internuclear distance, B_0 is the magnetic field strength, $\sigma_\parallel$ and $\sigma_\perp$ are the parallel and perpendicular components of the axially symmetric A-spin CSA tensor and $J(\omega)$ is the spectral density function. For calculations described herein r_{AX} was set to 1.02 Å and $\Delta\sigma = \sigma_\parallel - \sigma_\perp$ was set to − 160 ppm in the case of A = ^{15}N. The quantities d and c are coupling constants that are proportional to the static dipolar and chemical shift interactions, respectively, and the spectral densities, $J(\omega)$, are proportional to the amplitudes of the fluctuations in the dipolar and CSA interactions at frequency ω.

In the absence of dipolar cross-correlations, Equations (7.1)–(7.3) apply to methyl carbon relaxation, provided that $1/T_i$ ($i = 1, 2$) is replaced by $(1/3T_i)$. In this case $r_{AX} = 1.09$ Å and the CSA is neglected. A rotating methyl typically has $\Delta\sigma \leqslant 25$ ppm, from which one calculates that relaxation due to CSA is insignificant (less than 2.5%) compared with relaxation due to the dipolar interaction.

It was tacitly assumed in the above discussion that the pulse sequences used to measure the relaxation parameters eliminate cross-correlation between the dipolar and CSA interactions. Although this can be readily accomplished, RF pulses cannot completely eliminate the effects of cross-correlations among the three carbon–proton dipolar couplings in a methyl spin system. The effect of dipolar cross-correlation upon methyl carbon relaxation has been thoroughly investigated (Werbelow and Grant, 1977). In general, neither longitudinal nor transverse methyl carbon magnetization relaxes in a single exponential manner, and the equations for the NMR relaxation parameters become quite formidable. However, a recent analysis of these equations has shown that dipolar cross-correlations make only small contributions to longitudinal relaxation rates and to NOEs for carbons in rapidly rotating methyl groups in proteins. This is the case for two reasons. First, using the three-site Woessner model (Woessner, 1962) to describe methyl group internal dynamics, it is found that cross-correlation spectral density terms nearly vanish when the overall and the internal correlation times are in the 5–20 ns and 15–65 ps ranges, respectively (Kay and Torchia, 1991). Second, in larger proteins, efficient cross-relaxation involving methyl protons and neighbouring protons attenuates the effects of cross-correlation on T_1 measurements. If cross-correlation effects are significant, one can still apply Equation (7.1) provided that one derives the relaxation rate from the initial decay of the longitudinal magnetization.

In contrast with longitudinal relaxation, transverse methyl carbon relaxation is strongly affected by dipolar cross-correlations. Therefore, one must derive the T_2 value from the initial decay of the transverse magnetization (Werbelow and Grant, 1977). Finally, we note that chemical exchange may also contribute to the transverse relaxation rate in proteins, a subject that we discuss later in this review.

Model-free Formulation of Relaxation Equations

A useful way of expressing $J(\omega)$ in terms of the minimum number of model independent motional parameters is provided by the formalism of Lipari–Szabo (1982a,b). According to this formalism

$$J(\omega) = S^2\tau_m/(1 + (\omega\tau_m)^2) + (1 - S^2)\tau/(1 + (\omega\tau)^2) \quad (7.4)$$

where S is the generalized order parameter, τ_m is the overall correlation time and $1/\tau = 1/\tau_m + 1/\tau_e$, where τ_e is an effective correlation time characterizing the internal motions. Although Equation (7.4) contains a single effective internal correlation time, it is an exact expression for the spectral density function, even in the case of multiple internal motions, provided that all internal motions are in the extreme narrowing limit (Lipari and Szabo, 1982a), i.e. $(\omega\tau_i)^2 << 1$, where τ_i is the correlation time associated with an arbitrary internal motion.

Equation (7.4) applies to solids as well as to liquids. In solids, τ_m approaches infinity, and the first term in Equation (7.4) becomes vanishingly small. In this limit the expression for $J(\omega)$ becomes

$$J(\omega) = (1 - S^2)\tau_e/(1 + (\omega\tau_e)^2) \quad (7.5)$$

Equation (7.4) can be generalized to apply to the case when the internal motions take place on two (or more) significantly different time-scales, at least one of which is outside the extreme narrowing limit. For example, if two internal correlation times, τ_f and τ_s, are required to define the internal correlation function, $J(\omega)$ becomes (Clore *et al.*, 1990b)

$$J(\omega) = S^2\tau_m/(1 + (\omega\tau_m)^2) + (1 - S_f^2)\tau_f/(1 + (\omega\tau_f)^2) + S_f^2(1 - S_s^2)\tau_s/(1 + (\omega\tau_s)^2) \quad (7.6)$$

where S_f and S_s are the order parameters associated with the 'fast' and 'slow' internal motions and $S = S_fS_s$. Note that Equation (7.6) reduces to Equation (7.4) when $\tau_f = \tau_s$.

The physical interpretation of the model-free parameters is given in the next section, after discussion of how these parameters are derived from measured relaxation parameters.

3 Data Acquisition and Analysis

Pulse Sequences and Measurement Artifacts

In order to maximize resolution and sensitivity it is essential that heteronuclear (^{13}C or ^{15}N) relaxation parameters be measured by use of two-dimensional pulse schemes that employ proton detection (Kay *et al.*, 1989; Nirmala and Wagner, 1989). We discuss two classes of such experiments that are appropriate for AX and AX_3 spin systems, respectively.

Sequences for AX Spin Systems

Pulse sequences designed to measure the A-spin T_1, T_2 and NOE values in AX spin systems (typically A = ^{13}C or ^{15}N; X = ^1H) are depicted schematically in Figure 7.1. The sequences used to measure T_1 and T_2 (Kay *et al.*, 1992a; Palmer *et al.*, 1992) are improved versions of sequences proposed originally (Kay *et al.*, 1989) in that 180° ^1H pulses are applied periodically during the relaxation delay period, T, in order to suppress cross-correlation of AX dipolar coupling with A-spin CSA (Goldman, 1984; Boyd *et al.*, 1990). If this procedure is not followed, the amide ^{15}N relaxation times measured for SNase are overestimated by 5–9% in the case of SNase (Kay *et al.*, 1992b). Note that the T_1 and T_2 pulse sequences yield signals that decay to zero as the relaxation delay increases. Therefore, the relaxation measurement is independent of the delay time between scans, permitting the decay curve to be fitted with two parameters.

In order to measure the NOE of spin A, it is necessary to record spectra (a) with and (b) without proton saturation. The sensitivity of the NOE experiment is significantly below that of the T_1 and T_2 experiments (particularly when A = ^{15}N) because the initial magnetization must be derived from the A spins rather than from the protons. Furthermore, in contrast with the T_1 and T_2 experiments, it is necessary

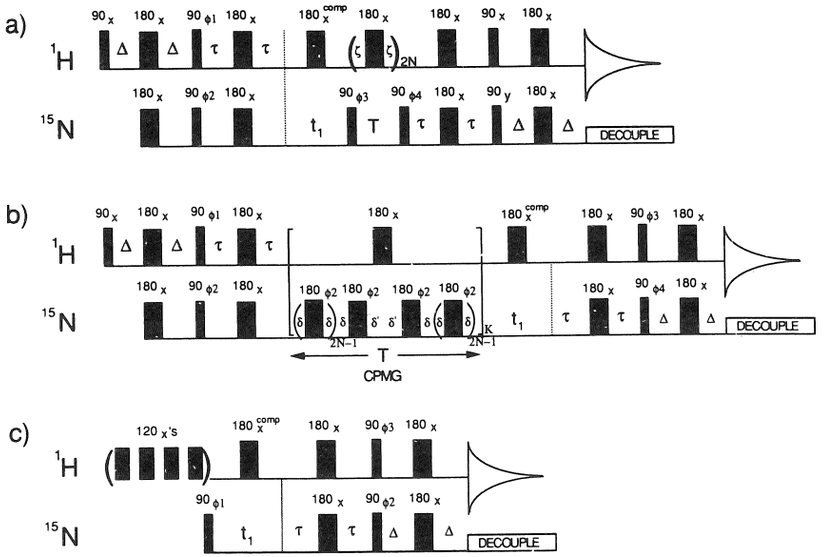

Figure 7.1 Pulse sequences used to measure (a) T_1, (b) T_2 and (c) the A-{^1H} NOE in AX spin systems. The sequences are discussed in detail in Kay *et al.* (1992a)

to wait a long period (> $3T_{1L}$, where T_{1L} is the larger of the proton and A-spin T_1 values) in order to ensure that AX cross-relaxation does not prevent the A-spin magnetization from attaining its equilibrium value prior to the application of the initial A-spin pulse. When experiments are recorded in H_2O, water saturation must be achieved quickly in the experiment without NOE, in order to minimize the transfer of saturation by spin diffusion. An alternative to presaturation in this experiment (Barbato *et al.*, 1992) is the application of a short scrambling sequence (Messerle *et al.*, 1989).

Pulse Sequences for AX_3 Spin Systems

Pulse sequences for measuring methyl ^{13}C relaxation parameters differ in a number of important ways from sequences used in an AX spin system. Sequences designed to measure ^{13}C relaxation parameters in methyl groups are shown in Figure 7.2. Note that, in contrast to the T_1 and T_2 sequences depicted in Figure 7.1, magnetization is initially derived from the heteronuclei rather than the protons. In our experience this causes no loss in sensitivity because (a) the NOE of the methyl carbons is large (typically in the range 2–2.5) and (b) at the cost of

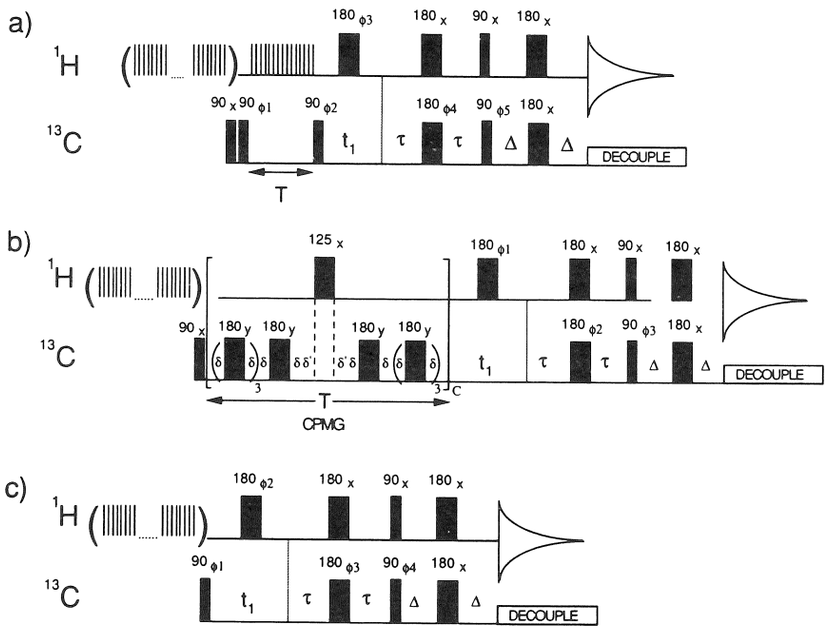

Figure 7.2 Pulse sequences used to measure (a) T_1, (b) T_2 and (c) the A-{^{1}H} NOE in AX_3 spin systems. The sequences are discussed in detail in Kay *et al.* (1992b)

reducing sensitivity, one must use magic angle pulses or delays in DEPT- and INEPT-type sequences, respectively, in order to suppress complicating effects that arise from dipolar cross-correlations (Palmer *et al.*, 1991b). Note that the delay time τ in the reverse INEPT portions of the T_1 and T_2 sequences in Figure 7.2(a,b) must satisfy the magic angle condition ($2\pi J\tau = 0.955 = 54.7°$) in order that magnetization be correctly transferred from ^{13}C transitions to proton transitions (Kay *et al.*, 1992a). Furthermore, the delay Δ is set to a short value, $1/(8J_{CH})$, so that rapid proton relaxation will not affect the measurement of the ^{13}C relaxation rates. These points and our reason for using the reverse INEPT rather than the reverse DEPT sequence are discussed in detail elsewhere (Kay *et al.*, 1992a). The sequences shown in Figure 7.2 have been tested (a) on [methyl-^{13}C]-leucine-labelled SNase and (b) on [methyl-^{13}C]-alanine, dissolved in deuterated glycerol, over a range of temperatures; they have been optimized to minimize artefacts when measuring methyl ^{13}C relaxation times in proteins by proton detection.

Although the pulse schemes in Figures 7.1 and 7.2 suppress cross-correlation of AX dipolar and A-spin CSA interactions, the pulse scheme in Figure 7.2(b) minimizes, but does not completely eliminate,

the effects of dipolar cross-correlations, because RF pulses do not mix the 3/2 and 1/2 proton manifolds (Ernst, 1966). Hence, the decay of transverse magnetization is biexponential, and the initial slope of the decay curve must be determined in order to measure T_2 correctly (Werbelow and Grant, 1977). Finally, we note that accurate T_2 values are obtained by the CPMG method only when the condition $\delta << 1/(2J)$ is satisfied (Kay *et al.*, 1989, 1992b; Peng *et al.*, 1991a). Because small values of δ are employed in the T_2 sequence, chemical exchange affects T_2 in almost the same manner as $T_{1\rho}$ (particularly because spin locking fields for heteronuclei in liquids are limited to < 10 kHz). Hence, it is difficult to find evidence for chemical exchange by comparing measured values of T_2 with $T_{1\rho}$. For reasons discussed elsewhere (Kay *et al.*, 1992a), we prefer to measure T_2 values using a CPMG-type sequence rather than to measure $T_{1\rho}$ values using a spin lock (Peng *et al.*, 1991b).

Relaxation Parameters and Their Uncertainties

In one-dimensional NMR experiments that employ heteronuclear detection, low sensitivity is the primary factor that limits the accuracy of the relaxation measurements in proteins. In addition to significantly enhancing resolution, proton-detected two-dimensional techniques greatly improve sensitivity. In the case of 1.5 mM solutions of SNase, typical signal-to-noise ratios are in the range of 50–100 for well-labelled samples (incorporation levels greater than 50%). At these signal-to-noise levels, the main uncertainty in determining the signal intensity arises from baseline distortions and from overlap of the signals of interest with the tails of nearby strong signals. With careful data processing, signal intensities can be measured with an accuracy of a few per cent. Signal intensities can be derived from measurements of either peak heights or peak volumes, with the latter quantities obtained from surface-fitting routines. The relaxation parameters derived from these two types of measurements should usually agree to within 5% or better.

In order to extract values of T_1 and T_2 from the NMR data, we measure the signal intensities of the cross-peaks in the 2D spectra recorded as a function of the relaxation delay, T, and fit the measured volumes to an equation of the form $y = A \exp(-t/T_i)$, using conjugate gradient minimization techniques (Press *et al.*, 1988). The standard deviations in the parameters A and T_i are derived from the residuals of the fits to the data by using a Monte Carlo approach (Kamath and Shriver, 1989; Nicholson *et al.*, 1992).

In a similar manner, NOE values are determined by measuring the signal intensities in the presence (I), and absence (I') of the NOE. The NOE is equal to the ratio I/I', while the error in the NOE measurement is given by

$$E(\mathrm{NOE}) = (I/I')[(\Delta I/I)^2 + (\Delta I'/I')^2]^{1/2} \quad (7.7)$$

where $\Delta I(\Delta I')$ is the error in the signal intensity measurement in the presence (absence) of the NOE. When signal intensity is obtained from peak height, the error is the standard deviation of the baseline noise. When signal intensity is obtained from a volume integral, the uncertainty is given by the standard deviation of the noise times the square root of the number of points in the area under integration.

Extracting Model-free Parameters from Relaxation Data

In analysing the relaxation data obtained on SNase, we assume that the overall (rigid body) reorientation of the molecule is isotropic and is characterized by a single correlation time, τ_m. This assumption is validated by (a) the fact that the principal components of the inertia tensor of the protein are calculated (using the crystal coordinates) to be in the ratio of 1.0:1.3:1.4, and (b) by the observation that the amide ^{15}N T_1/T_2 ratio is nearly the same (rms variation of 6%) for all residues in the protein.

In addition to their dependence on the global parameter τ_m, the relaxation parameters depend upon the residue-specific model-free parameters S and τ_e. A general approach to determine these three parameters consists of minimizing the error function (Dellwo and Wand, 1989)

$$E = \sum_i \{[(T_{1i}^{\mathrm{obs}} - T_{1i}^{\mathrm{cal}})/T_{1i}^{\mathrm{obs}}]^2 + [(T_{2i}^{\mathrm{obs}} - T_{2i}^{\mathrm{cal}})/T_{2i}^{\mathrm{obs}}]^2 + [(\mathrm{NOE}_i^{\mathrm{obs}} - \mathrm{NOE}_i^{\mathrm{cal}})/\mathrm{NOE}_i^{\mathrm{obs}}]^2\} \quad (7.8)$$

The minimization is carried out by assigning a value of τ_m to all residues in the protein, and then determining the set of $\{S_i, \tau_{ei}\}$ that minimize E, using conjugate gradient minimization. This process is repeated, stepping τ_m through a series of values until the minimum value of E is determined.

A Monte Carlo procedure (Kamath and Shriver, 1989) is used in order to ascertain the precision limits on the derived values of $\{S_i, \tau_{ei}\}$. Having determined the values and standard deviations of the NMR relaxation parameters (T_1, T_2 and the NOE) as described in the previous section, a Gaussian random number generator is used to generate synthetic values of these parameters, and the error function defined in Equation (7.8) is minimized with respect to S_i, and τ_{ei}. This procedure is repeated for several hundred synthetic data sets in order to determine the distribution of values of the model-free parameters. These distributions are used to derive uncertainties in the model-free parameters.

While the procedure outlined above for determining the values and precision limits of the model-free parameters is generally applicable, a few practical comments are perhaps in order. When measuring backbone relaxation parameters, the investigator should note whether the NOEs are close to their slow motion values. If this is the case, then the $\tau_e = 0$ approximation is valid (Kay *et al.*, 1989). This permits a simpler two-parameter, τ_m, S, fit of the data to be made. The investigator should also note whether a residue has an anomalously small backbone T_2 value, as this is strong evidence that chemical exchange makes a significant contribution to T_2; hence, the relaxation parameters for this residue should be excluded from Equation (7.8). At the other extreme, if a residue has an anomalously large T_2 value and an NOE value significantly different from the slow tumbling limiting value, it is possible that the residue exhibits a complex segmental motion that cannot be simply described by a single internal correlation time. For this reason the relaxation parameters for such a residue should be excluded from Equation (7.8). Once the optimum value of τ_m is determined, the relaxation parameters obtained for the flexible residue can be used to determine the values of τ_m, S and τ_e. If the optimum model-free parameters do not yield calculated relaxation parameters that agree with experiment, then a more complex analysis involving two internal order parameters and correlation times is warranted (Clore *et al.*, 1990b). One must be particularly careful about analysis of ^{15}N relaxation times of flexible residues, because the relaxation parameters of these residues may be affected by rapid exchange of the amide protons with solvent water molecules. Although we have assumed that the overall motion of the protein is isotropic (since this is appropriate in the case of SNase), this assumption is not a requirement of the model-free approach, and methods for dealing with anisotropic motion have been described (Lipari and Szabo, 1982a,b; Dellwo and Wand, 1989; Barbato *et al.*, 1992).

Deriving Motional Information from Model-free Parameters

The overall correlation time derived from the model-free approach, τ_m, can be compared with values calculated by hydrodynamic theory (Venable and Pastor, 1988). The correlation time of a sphere with volume V in a medium having viscosity η is given by

$$\tau_m = \eta V/kT \quad (7.9)$$

where k is Boltzmann's constant and T is the absolute temperature. It is necessary to use a 3 Å hydration sphere in order to bring the values of τ_m calculated from Equation (7.9) into agreement with values of τ_m measured by NMR techniques. The value of τ_m obtained from Equation (7.9) (including the 3 Å hydration layer) is sometimes less than the value of τ_m obtained from ^{15}N NMR relaxation measurements. At present the reason for this discrepancy is not clear, but may be a consequence of

the high protein concentrations (*c.* 20–30 mg/ml) typically required for NMR studies.

The bulk of the information obtained from NMR experiments is contained in the residue-specific parameters S and τ_e. Although τ_e provides an estimate of the time-scale of the internal motion, it is difficult to interpret this parameter in a quantitative fashion, because it is a complex combination of geometric factors and internal correlation times (Lipari and Szabo, 1982a,b). In contrast, the generalized order parameter is precisely related to the equilibrium orientational distribution function associated with internal motions having correlation times that are smaller than the overall correlation time of the protein. When the NMR interaction responsible for spin relaxation is axially symmetric with the unique axis parallel to the AX bond vector (a condition that is rigorously satisfied by the AX dipolar interaction and is approximately true for the CSA interaction considered herein), the generalized order parameter is given by the expression (Lipari and Szabo, 1982a)

$$S^2 = \int d\Omega_1 p_{eq}(\Omega_1) \int d\Omega_2 p_{eq}(\Omega_2)\, P_2(\cos\theta_{12}) \tag{7.10}$$

where $p_{eq}(\Omega)d\Omega$ is the normalized equilibrium probability that the vector $\boldsymbol{\mu}$, a unit vector along the AX bond axis, has orientation $d\Omega$, $\Omega = (\theta, \phi)$, in a coordinate system fixed in the protein, θ_{12} is the angle between two such vectors, $\hat{\boldsymbol{\mu}}_1$ and $\hat{\boldsymbol{\mu}}_2$, and $P_2(\cos x) = (3\cos^2 x - 1)/2$. Using Equation (7.10), one can calculate S for any model of AX bond reorientation. For instance, in the cone model, where $\hat{\boldsymbol{\mu}}$ diffuses freely in the angular region $0 < \theta < \theta_0$, $0 < \phi < 2\pi$, one finds that

$$S^2 = [(1/2)\cos\theta_0(1 + \cos\theta_0)]^2 \tag{7.11}$$

This expression reveals several general features about the relationship of the order parameter with the amplitude of the motion. The order parameter equals unity in the absence of motion, $\theta_0 = 0$, diminishes as θ_0 increases, vanishing when motion is isotropic, $\theta_0 = 180°$. Note, however, that S^2 is not a monotonic function of θ_0. It vanishes even when motion is not isotropic, i.e. $\theta_0 = 90°$, and attains a small local maximum at $\theta_0 = 120°$. In general, a small-amplitude motion implies that S^2 is large. However, a large-amplitude motion need not have a small order parameter. For example, if the AX bond reorients by jumps of 180°, $S^2 = 1$.

The order parameter is closely related to the orientation-dependent local magnetic fields (due to either dipolar coupling or CSA) that are responsible for relaxation. In the absence of reorientation, these local fields are the sources of the static powder line shapes observed in the spectra of unoriented solid samples (Haeberlen, 1976). The size of the local magnetic field parallel to the external field determines the width of the powder line shape, which is normally characterized by principal frequencies or equivalently by moments. In the presence of motion, the line shape narrows and the moments are reduced. The ratio between the motionally averaged second moment and the static second moment is proportional to S^2 (Torchia and Szabo, 1985). S^2 is therefore proportional to the value of the mean squared local field that remains after motional averaging.

In addition to the cone model, several other plausible models of internal motion have proved useful in analysing relaxation data. These models are now briefly described and expressions for their corresponding order parameters are given.

The Restricted Diffusion Model

If the unit vector $\hat{\boldsymbol{\mu}}$, along the AX bond axis, makes an angle of 109.5° with a rotation axis and undergoes rotational diffusion (about the axis) through an angular range of $\pm\gamma_0$, S^2 is given by

$$S^2 = (1/9)[1 + 8\sin^2\gamma_0(1 + 2\cos^2\gamma_0)/(3\gamma_0^2)] \tag{7.12}$$

The Two-site Jump Model

If $\hat{\boldsymbol{\mu}}$ abruptly changes its orientation by 109.5°, S^2 is given by

$$S^2 = 1 - (8/3)[r/(1 + r)^2] \tag{7.13}$$

where $r = p_1/p_2$, and p_1 and p_2 are the relative populations of the two orientations of $\hat{\boldsymbol{\mu}}$.

Threefold Rotation

If $\hat{\boldsymbol{\mu}}$ reorients about a threefold axis, S^2 is given by

$$S^2 = [(3\cos^2\theta - 1)/2]^2 \tag{7.14}$$

where θ is the angle between $\boldsymbol{\mu}$ and the rotation axis.

4 Applications

SNase Backbone Dynamics in Solution

Using the pulse sequences described in Figure 7.1, backbone amide ^{15}N T_1, T_2 and NOE values were measured for *c.* 100 of the 149 amino acid residues in liganded SNase (complexed with pdTp and Ca^{2+}). The

T_1 and T_2 values are plotted as a function of residue number in Figure 7.3. The relaxation times of the SNase sample measured using the sequences in Figure 7.1 are 5–10% shorter than the relaxation times measured using sequences reported previously (Kay *et al.*, 1989), because the original sequences did not entirely eliminate the effects of cross-correlation of dipolar and CSA interactions. The first six residues and

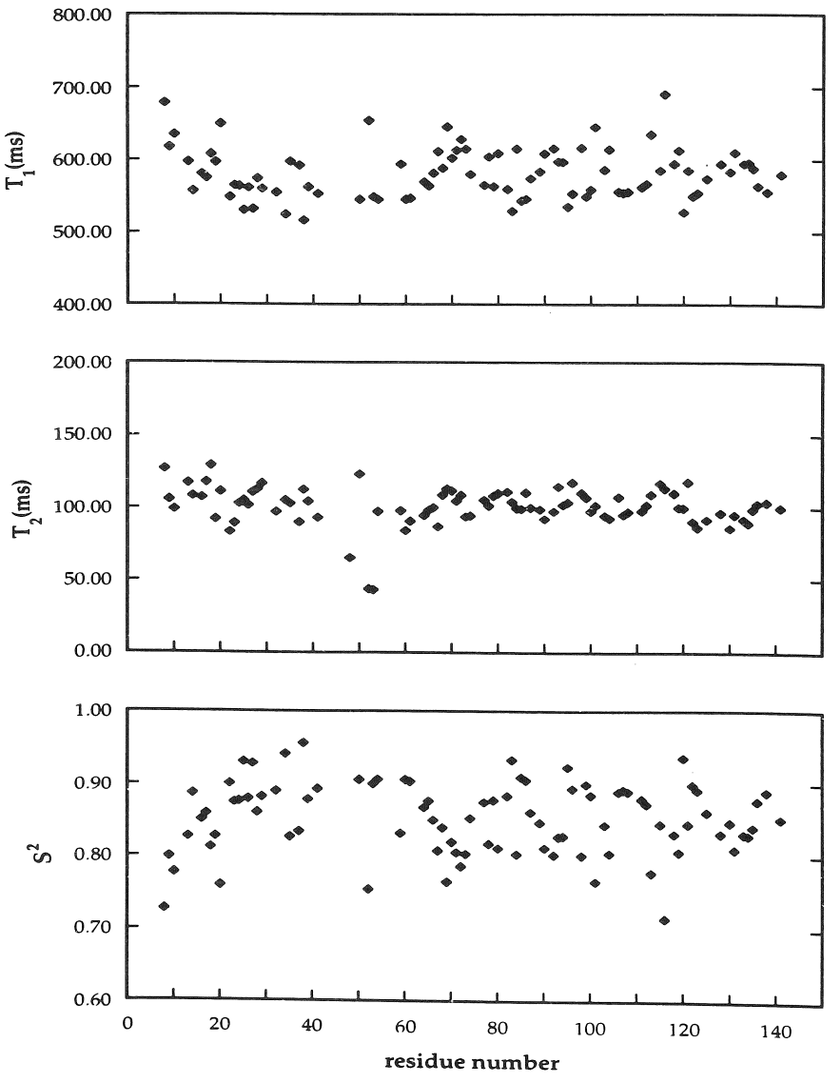

Figure 7.3 Amide ^{15}N T_1, T_2 and S^2 values obtained for the various residues of SNase

the last eight residues in SNase are not included in Figure 7.3, because the amide protons of these residues exchange rapidly with water. In addition, relaxation times were not obtained for a number of residues in or near the disordered Ω loop of SNase (Baldisseri *et al.*, 1991), because their signals were severely exchange broadened. The remaining residues not included in Figure 7.3 are either prolines or residues whose NMR signals are not well enough resolved to permit accurate measurements of their relaxation times.

As noted previously (Kay *et al.*, 1989), because the NOE values for all residues (except for the flexible residues in the N and C termini of the protein) are nearly equal to their slow limit ($(\omega_A\tau_m)^2 >> 1$) value of 0.82, the $\tau_e = 0$ approximation is valid and Equations (7.1) and (7.2) can be replaced by the simple expressions

$$1/T_i = S^2(1/T_i)_{abs} \tag{7.15}$$

where $i = 1,2$, and the subscript 'abs' indicates the value of the relaxation time in the absence of internal motion. Following Kay *et al.* (1989), we calculate τ_m on a residue-by-residue basis from the T_1/T_2 value for each residue, and then calculate the value of τ_m for SNase as the average of values obtained for all the residues. In this manner we obtain $\tau_m = 8.3 \pm 0.5$ ns for SNase, slightly less than the value of 9.1 ns reported previously, using relaxation times measured in the presence of dipolar/CSA cross-correlations. Three residues in the Ω loop region of SNase (K48, E52 and K53) were excluded from the calculation of the average τ_m value because they have anomalously small T_2 values, which indicates that chemical exchange makes a significant contribution to their T_2 values. In addition, the flexible terminal residues were excluded from the calculation of τ_m because their NOE values indicated that $\tau_e = 0$ was not a good approximation for these residues.

Having determined τ_m, S^2 is obtained for each residue, using Equation (7.1) or (7.2), respectively, with either the T_1 or T_2 value measured for the residue. The values of S^2 obtained in this manner, using the measured T_1 values (Figure 7.3), are in good agreement (rms difference 0.035) with those reported previously (Kay *et al.*, 1989).

It is evident from the figure that T_1 values and the corresponding values of S^2 do not show a large variation from residue to residue. This is also true of the T_2 values, except for those residues in the disordered Ω loop. As noted above, these residues have exceptionally small T_2 values but their T_1 and NOE values are close to the average values of these parameters observed for the other residues in SNase. Hence, it appears that relatively slow chemical exchange, $\tau_{exch} \approx 10^{-4}$–$10^{-6}$ s, modulation of amide chemical shifts is responsible for the small T_2 values of these residues.

The observation that the values of S^2 are rather uniform, $\langle S^2 \rangle = 0.85 \pm 0.05$, should not be taken to mean that the high-frequency backbone motions are homogeneous throughout SNase. Using the cone model and Equation (7.11) to estimate the amplitudes of the internal motions, one finds that θ_0 increases from 10.5° to 22° as S^2 decreases from 0.95 to 0.80. Hence, a decrease in S^2 of 15% corresponds to a fourfold increase in the solid angle through which the NH bond reorients.

Unfortunately, one cannot conclude from these remarks that the observed variations in S^2 are a consequence of differences in the amplitudes of the internal motions of the NH bonds. In SNase where the $\tau_e = 0$ approximation is valid, it is easy to show that, to a good approximation, the relaxation rates are proportional to $S^2\langle r_{NH}^{-3} \rangle^2$. Hence, a 13% variation in relaxation rate (and in S^2) would result from a 0.02 Å variation in NH bond length. For this reason, most of the observed variation in S^2 could result from small differences in the NH bond lengths.

Note that in the solid state, where the spectral density is totally determined by the internal motion (Equation 7.5), the relaxation rate in the extreme narrowing limit is proportional to $(1 - S^2)\tau_e\langle r_{NH}^{-3} \rangle^2$. One sees that the relaxation rate increases threefold as S^2 decreases from 0.95 to 0.8. Hence, these considerations suggest that one could detect heterogeneity in SNase backbone dynamics by measuring ^{15}N amide T_1 values in the crystalline protein.

SNase Backbone Dynamics in the Crystalline State

The cross-polarization magic angle sample spinning, CPMASS, spectrum of crystalline SNase labelled with [^{15}N]-valine (Figure 7.4), shows eight resolved signals, whose chemical shifts nearly coincide with the chemical shifts of sequentially assigned valine signals observed in solution. The close coincidence of chemical shifts observed in solution with shifts observed in the solid-state spectrum permits sequential assignment of signals in the solid-state spectrum of all residues except Val 51. This residue is in the disordered Ω loop of SNase, and its signal is not observed in the CPMASS spectrum, because it is presumably broadened by molecular motion. The spin–lattice relaxation rates of the eight observed valine signals were measured at 5.9 and 11.7T, and are compared with the corresponding solution state measurements in Figure 7.5. The figure shows that relaxation rates observed in solution are nearly 100 times larger than those observed in the crystalline state. This result is a consequence of the fact that, in solution, the overall motion of SNase is primarily responsible for relaxation of the backbone amide ^{15}N spins, whereas in the solid phase relaxation is due exclusively to small-amplitude internal motions. As anticipated above, Figure 7.5 also

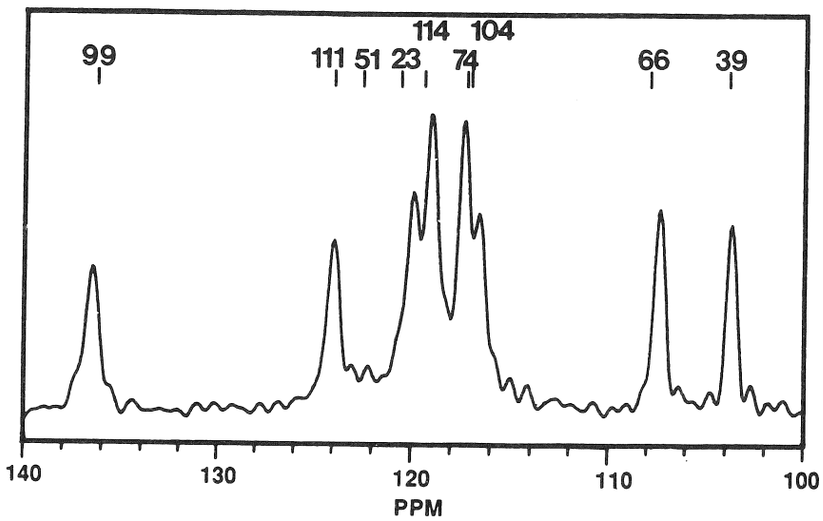

Figure 7.4 CPMASS spectrum of crystalline SNase labelled with [^{15}N]-valine. Resonance positions and signal assignments obtained in solution are indicated at the top of the figure

shows that the spin–lattice relaxation rates of the various valine residues show a much greater variation in the solid state than in solution.

Spin–lattice relaxation rates were also recorded at 5.9T for crystalline SNase labelled with ^{15}N His, and the relaxation rates of the His and Val residues are plotted against the X-ray temperature factors in Figure 7.6. While the plot shows that the relaxation rate increases as the order parameter increases, the correlation is by no means perfect. This is expected because B values contain contributions from static disorder, and from motions on a time-scale ranging from ps to the time required to collect the diffraction data. In addition, Equations (7.1) and (7.5) show that the relaxation rate depends upon a product, $(1 - S^2)\tau_e$, involving both the relaxation time and the internal correlation time. Hence, the measured relaxation time will reflect both the rate as well as the amplitude of the internal motion.

Although it is in principle possible to derive S^2 from measurements of spinning sidebands observed in CPMASS spectra (Cole and Torchia, 1991), signal-to-noise limitations as well as uncertainties in the static values of the ^{15}N CSA tensor elements limit the accuracy of such measurements to an uncertainty of 10%. It is also possible to determine τ_e from field-dependent T_1 measurements. However, the small field dependence that is observed implies that the derived τ_e value is extremely sensitive to uncertainties in the T_1 values (Cole and Torchia, 1991). The

very large values of T_1 observed in the solid state limit the accuracy of the T_1 measurements to *c.* 10%, thus precluding a precise determination of the internal correlation time.

While it is not possible to distinguish the separate contributions of the order parameter and the internal correlation time to the spin–lattice

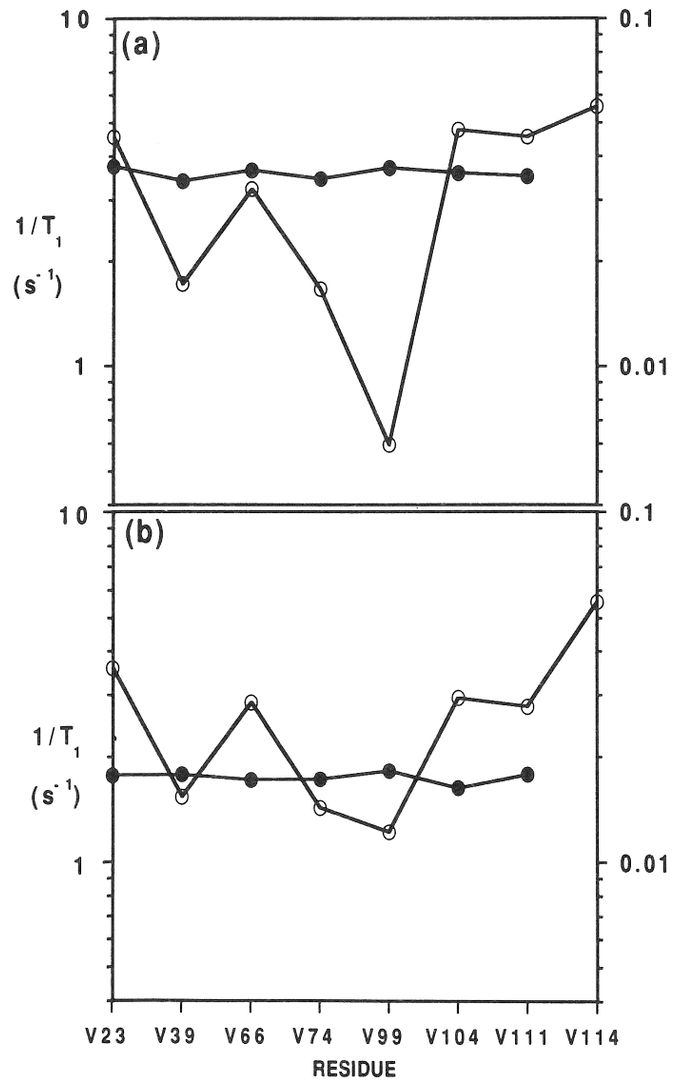

Figure 7.5 Comparison of SNase [^{15}N-Val spin–lattice relaxation rates measured in solution (●) and in the crystalline state (○) at (a) $6T$ and (b) $12T$

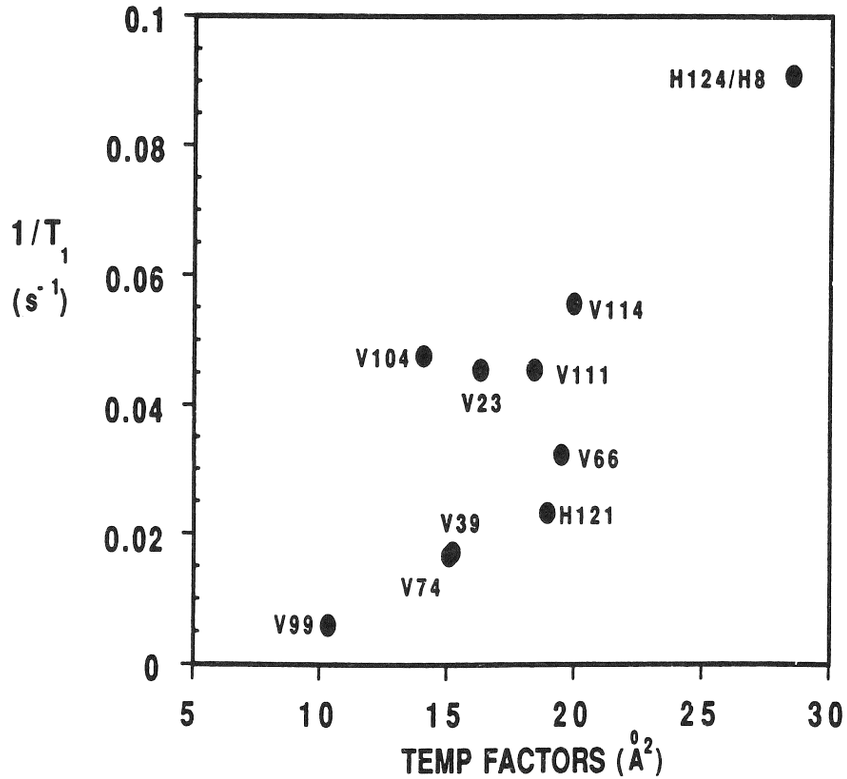

Figure 7.6 Comparison of X-ray B factors and spin–lattice relaxation rates of SNase measured in the crystalline state at $6T$

relaxation in the crystalline phase, it is clear that the variation in the measured T_1 must arise because of variations of one or both of these motional parameters from one residue to another. That is, the variations in the measured T_1 values are a consequence of heterogeneity in the internal motion of the protein backbone. It will thus be interesting to see whether these variations in internal dynamics of individual residues in SNase can be reproduced by molecular dynamics calculations.

Internal Dynamics of SNase Leucine Side-chains in Solution

We have seen that with the exception of a few amino acids in the N and C termini, and in the Ω loop of the protein, the internal motions of the backbone NH bond vectors are restricted to small-amplitude fluctuations. It is to be expected that internal motions of the amino acid side-chains, particularly those at or near the protein surface, will execute

motions of considerably larger amplitude. Clear evidence for such motions are the narrow linewidths typically observed for the signals arising from the side-chains of Lys and Arg residues in proteins. Although one expects that motions of large hydrophobic residues will be considerably more restricted because they are usually buried within the protein, pioneering studies of methyl carbons in myoglobin (Wittebort *et al.*, 1979) and BPTI (Richarz *et al.*, 1980) suggested that a number of large hydrophobic side-chains in these proteins had significant internal motions in addition to rotation of the methyl group. Also, ^{2}H NMR studies of crystalline SNase showed that the side-chains of the Met and Phe residues experienced large-amplitude motions (Sparks *et al.*, 1989).

Until recently a major impediment to the study of side-chain dynamics in proteins has been the absence of sequential signal assignments. However, isotopic enrichment combined with multidimensional NMR spectroscopy now provides a method for obtaining nearly complete assignments of protons and heteronuclei of proteins in the 15–25 kDa range (Clore *et al.*, 1990a; Ikura *et al.*, 1991; Pelton *et al.*, 1991). In addition, this methodology provides spectra having high sensitivity and resolution. For example, the proton-detected HMQC spectrum of SNase/pdTp/Ca^{2+} labelled with [5,5′-^{13}C]-leucine (Figure 7.7) shows 22 resolved methyl signals corresponding to the 11 leucine residues in the protein. These signals were sequentially assigned, using a variety of two- and three-dimensional experiments (Nicholson *et al.*, 1992), as were the corresponding signals of SNase in the absence of ligands. Stereospecific assignments were obtained by comparing NOE patterns predicted by the crystal structure of the protein (Loll and Lattman, 1989; Hynes and Fox, 1991) with those observed in NMR spectra. This procedure is justified, since all available evidence indicates that the crystal and solution structures of SNase backbone and buried side-chain atoms are essentially the same (Torchia *et al.*, 1989; Wang *et al.*, 1990a,b; Baldisseri *et al.*, 1991).

Although nearly all of the leucine methyl groups in SNase are completely buried, the previous evidence that buried hydrophobic groups in proteins exhibit internal flexibility encouraged us to measure ^{13}C relaxation parameters in order to investigate the dynamics of these methyl groups in SNase. The T_1, T_2 and NOE values of all 22 methyl carbons were measured, using the pulse sequences diagrammed in Figure 7.2 (Nicholson *et al.*, 1992).

Model-free parameters were extracted from the relaxation data (Nicholson *et al.*, 1992) in two different ways. First, the values of τ_m, S^2 and τ_e were derived from the relaxation data, using Equation (7.8). This approach yielded values of τ_m of 6.6 ns and 7.2 ns for liganded and unliganded SNase, respectively. These values are significantly smaller than the values of 8.3–8.5 ns obtained from measurements of backbone

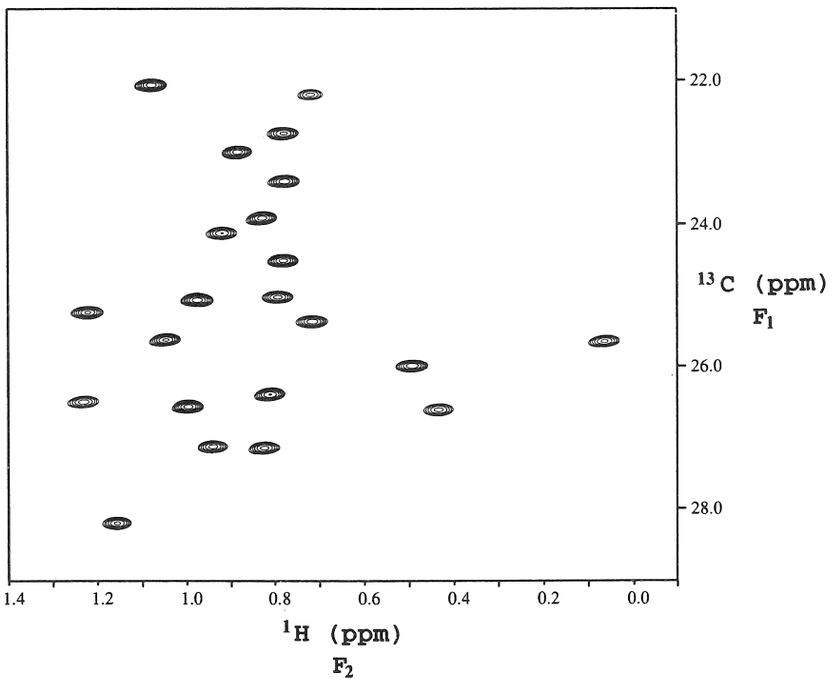

Figure 7.7 Two-dimensional shift correlation spectrum of SNase labelled with [5,5′-$^{13}C_2$]-leucine, showing the 22 resolved methyl signals of the 11 Leu residues

relaxation parameters. In addition, the NOE values predicted by the best-fit values of the model-free parameters were, in general, 10–15% larger than the experimental NOEs. These differences are well outside the 1–2% errors estimated for the NOE measurements.

We think that these inconsistencies arise because not all internal motions of the methyl group are in the extreme narrowing limit. Physical considerations suggest that in addition to rapid threefold rotation of the methyl group, a motion of the C^γ–C^δ bond axis on a slower time-scale also occurs. The order parameters and effective correlation times associated with the fast (methyl rotation) and slow (C^γ–C^δ bond axis reorientation) internal motions are designated S_f, S_s, τ_f and τ_s, respectively. The spectral density function, $J(\omega)$, is given in terms of these parameters and τ_m in Equation (7.6). In order to extract the model-free parameters from the relaxation data, we set τ_m equal to 8.5 ns and note that, according to Equation (7.14), $S_f^2 = 0.111$ for a methyl group having tetrahedral geometry and rotating about its threefold axis. With the values of τ_m and S_f^2 set equal to 8.5 ns and 0.111, respectively, the remaining model-free parameters, S_s, τ_s and τ_f, were determined for each

leucine methyl carbon, from conjugate gradient minimization of Equation (7.8), and are listed in Table 7.1. For purposes of comparison, the values of the slow internal motion order parameters, S_{LZ}^2, are listed. These order parameters are obtained by dividing the squared order parameter derived using the original Lipari–Szabo formulation ($J(\omega)$ is given by Equation 7.5) by 0.111. Examination of the table shows that S_s^2 and S_{LZ}^2 typically differ by less than 5%.

Table 7.1 Effective correlation times[a] obtained for fast internal motions, τ_f, and the order parameters[b], S_s^2 and S_{LZ}^2, of leucine methyl carbons

		Liganded SNase					*Unliganded SNase*				
Carbon		τ_f	S_s^2	*Error*	S_{LZ}^2	*Error*	τ_f	S_s^2	*Error*	S_{LZ}^2	*Error*
L7	δ1	0.032	0.591	0.048	0.631	0.060	0.026	0.449	0.031	0.478	0.038
	δ2	0.034	0.466	0.022	0.479	0.023	0.047	0.518	0.040	0.524	0.031
L14	δ1	0.040	0.727	0.048	0.706	0.052	0.037	0.717	0.028	0.707	0.023
	δ2	0.053	0.890	0.028	0.885	0.034	0.058	0.887	0.036	0.897	0.043
L25	δ1	0.014	0.891	0.054	0.878	0.023	0.022	0.777	0.052	0.754	0.056
	δ2	0.029	0.815	0.028	0.906	0.025	0.035	0.910	0.039	0.898	0.041
L36	δ1	0.053	0.463	0.036	0.527	0.023	—	—		—	
	δ2	0.026	0.516	0.013	0.533	0.015	0.024	0.369	0.023	0.379	0.025
L37	δ1	0.083	0.958	0.030	0.955	0.028	0.049	0.640	0.088	0.725	0.028
	δ2	0.054	0.819	0.051	0.840	0.034	0.032	0.601	0.021	0.629	0.014
L38	δ1	0.014	0.697	0.061	0.755	0.029	0.023	0.502	0.037	0.506	0.042
	δ2	0.016	0.602	0.025	0.612	0.028	0.015	0.381	0.023	0.401	0.022
L89	δ1	0.034	0.840	0.031	0.881	0.024	0.029	0.577	0.085	0.667	0.021
	δ2	0.005	0.916	0.030	0.980	0.014	0.005	0.654	0.037	0.792	0.023
L103	δ1	0.040	0.881	0.038	0.878	0.029	—	—		—	
	δ2	0.060	0.931	0.039	0.913	0.044	0.065	0.688	0.037	0.806	0.050
L108	δ1	0.025	0.806	0.051	0.803	0.036	0.035	0.787	0.057	0.788	0.040
	δ2	0.028	0.884	0.036	0.855	0.027	0.027	0.757	0.046	0.840	0.033
L125	δ1	0.034	0.516	0.018	0.523	0.022	0.059	0.331	0.041	0.319	0.038
	δ2	0.014	0.441	0.018	0.451	0.022	0.038	0.373	0.012	0.364	0.014
L137	δ1	0.024	0.612	0.045	0.630	0.027	0.024	0.570	0.056	0.640	0.048
	δ2	0.025	0.522	0.011	0.544	0.011	0.023	0.443	0.050	0.491	0.045

[a] In ns.

[b] The values of S_f^2 are assumed to equal 0.111 and τ_m is 8.5 ns. The slow-motion order parameter obtained using the Lipari–Szabo analysis, Equation (7.3) divided by 0.111, S_{LZ}^2, is listed to allow comparison with S_s^2. The stereospecific assignments for L14, L103 and L137 are reversed from those published previously (Nicholson *et al.*, 1992). The previous assignments were based upon the crystal structure in an early stage of refinement.

Probably the major source of uncertainty in determining S_s^2 is the sensitivity of S_f^2 to the geometry of the methyl group. The methyl geometries determined from neutron diffraction studies of single crystals of L-alanine and L-valine are not ideal tetrahedral; rather they correspond to S_f^2 values of 0.104, 0.085 and 0.090. If the value of S_f^2 used to calculate the results in Table 7.1 had been 0.090 rather than 0.111,

the S_s^2 values would be 20% larger, with several sites having physically unreasonable order parameters in excess of unity. In view of this result and the fact that the strong ionic forces present in the crystals of amino acids may slightly distort the geometry of the methyl group, we have chosen to analyse the dynamics of the Leu methyl groups assuming tetrahedral geometry, recognizing that the values of S_s^2 so obtained have uncertainties of 10–20% as a consequence of possible variations in methyl group geometry.

Examination of Table 7.1 reveals that the values of S_s^2 show significant variation from residue to residue. Figure 7.8 shows a plot of the values of S_s^2 against the X-ray temperature factors obtained for liganded (Loll and Lattman, 1989) and unliganded (Hynes and Fox, 1991) SNase. There is an evident correlation between the order parameters and *B* values, although, for the reasons mentioned when discussing Figure 7.6, it is imperfect. An interesting feature of the Leu temperature factors is that, in a given residue, they are not significantly larger for the side-chain methyl carbons than for the backbone atoms. A comparison of Figure 7.3 and Table 7.1 shows that this result is in accord with the observation that the order parameters of the amide groups of L14, L25, L37, L89, L103 and L108 in liganded SNase are approximately the same

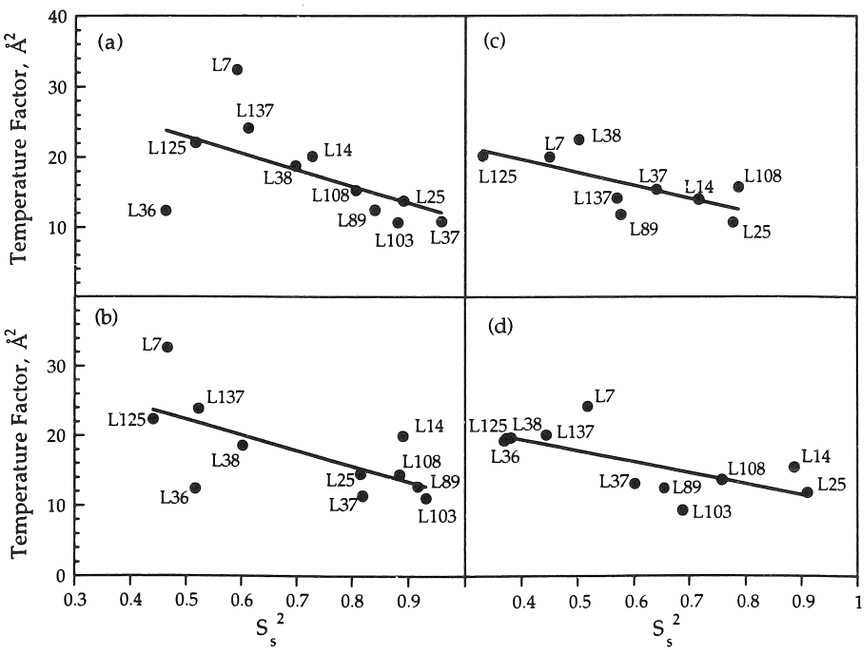

Figure 7.8 Plot of S_s^2 against the X-ray B factors for leucine δ_1 and δ_2 carbons of (a), (b) liganded and (c), (d) unliganded SNase

as the order parameters of the methyl carbons. In contrast, the order parameters of the methyl carbons of residues L36, L38, L125 and L137 are significantly smaller (S_s^2 is less than 0.71 for each residue) than the order parameters of their corresponding amide NH groups. This result is interesting, as it suggests that buried side-chains in liganded SNase undergo significant internal motions. We note that in the case of L7, the first residue in the ordered structure of SNase, the backbone amide S^2 has a low value of 0.54 (Kay *et al.*, 1989). However, the L7 side-chain is buried and has *B* factors (Figure 7.8) only slightly larger than those of the other Leu methyl carbons. We therefore also interpret the small order parameters observed in the case of the L7 methyl carbons in terms of internal motions of the buried L7 side-chain.

The values of the Leu methyl order parameters decrease further in the case of the unliganded protein (Table 7.1), with the result that, in addition to the five residues listed above, L37, L89 and L103 also have values of S_s^2 less than 0.7. Because the order parameters of the δ_1 and δ_2 carbons of each leucine side-chain are nearly the same (Table 7.1), the average order parameter of each pair is plotted in Figure 7.9. In order to compare the flexibility of the Leu side-chains in the liganded and unliganded states, we analyse the order parameters in terms of the following three specific models of internal motion of the Leu side-chains: (1) the cone model, in which the C^γ–C^δ bond axis diffuses in a cone of semiangle θ_0; (2) the restricted-diffusion model, in which the C^β–C^γ

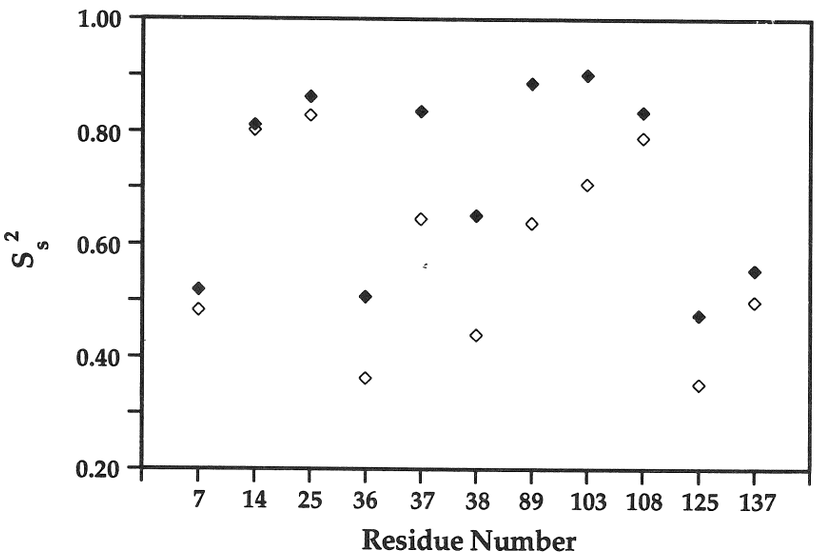

Figure 7.9 Plot of average S_s^2 for each pair of methyl groups in the presence (◆) and absence (◇) of ligands

bond axis diffuses through an angular range $\pm\gamma_0$; and (3) the two-site jump model, in which the C^γ–C^δ bond axis is found in one of two orientations that differ by 109.5°. In this latter model, the equilibrium probabilities of the two orientations are p_1 and p_2, with $r = p_1/p_2$, and the bond axis executes instantaneous jumps between the two orientations.

The values of θ_0, γ_0 and r derived from the measured ordered parameters and Equations (7.11)–(7.13) are listed in Table 7.2. Examination of the table shows that the flexible leucine side-chains, i.e. those for which $S^2 < 0.7$, undergo internal motions of significant angular amplitude in the case of either the cone or the restricted-diffusion model. Alternatively, in the case of the two-site jump model, where the angular amplitude is fixed to a large value, the minor conformation has a significant probability of occupation. Hence, about half of the buried leucine side-chains in SNase exhibit significant internal motions.

Table 7.2 Values of S_s^2 and corresponding values of θ_0, γ_0 and r derived from the cone, restricted diffusion and two-site jump models of leucine side-chain motion, respectively, in liganded (L) and unliganded (U) SNase

Residue		S_s^2	θ_0	γ_0	r
L7	(L)	0.53	36°	50°	0.30
	(U)	0.48	39°	54°	0.36
L36	(L)	0.49	38°	53°	0.35
	(U)	0.37	45°	65°	0.62
L37	(L)	0.89	16°	21°	0.05
	(U)	0.62	32°	43°	0.21
L38	(L)	0.65	30°	41°	0.18
	(U)	0.44	41°	58°	0.43
L89	(L)	0.88	17°	22°	0.05
	(U)	0.62	32°	43°	0.21
L103	(L)	0.91	14°	19°	0.04
	(U)	0.69	28°	38°	0.16
L125	(L)	0.48	39°	54°	0.36
	(U)	0.35	46°	67°	0.73
L137	(L)	0.57	34°	47°	0.25
	(U)	0.50	38°	52°	0.33

Another interesting feature of Table 7.2 is the evident difference in internal motion of the leucine side-chains in the liganded and unliganded proteins. Examination of Table 7.2 shows that the six leucine side-chains identified with an asterisk in Figure 7.10 (L36, L37, L38, L89, L103 and L125) show a significant decrease in internal flexibility in the presence of ligands. According to the crystal structure of liganded SNase (Loll and Lattman, 1989), the C^δ atoms of these six residues are within 10 Å

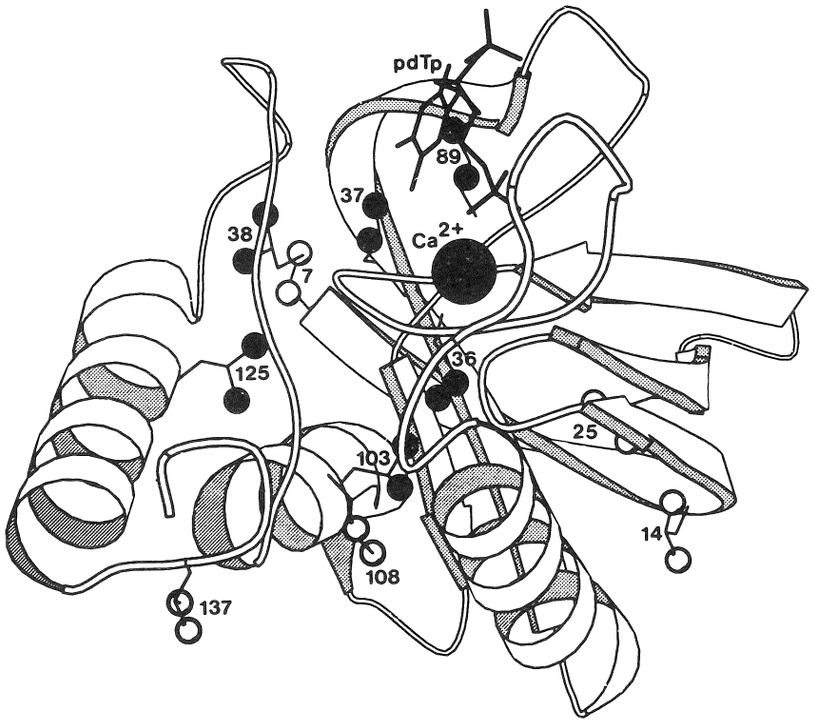

Figure 7.10 Structure of liganded SNase, showing the positions of the 11 pairs of leucine methyl carbons

of either Ca^{2+} or at least one of the heavy atoms of pdTp, while the C^{δ} atoms of the remaining five leucine residues are not.

The greater mobility of the leucine side-chains in unliganded SNase was not expected *a priori*. The comparison of the X-ray structures of liganded (Loll and Lattman, 1989) and unliganded (Hynes and Fox, 1991) SNase show relatively few differences in protein conformation, and these are confined to the protein surface near the ligand binding sites. It is true that the liganded protein undergoes thermal unfolding at a temperature 12–20° higher than unliganded SNase, and that the slowly exchanging amide protons have rates that are 2–3 orders of magnitude slower in the liganded protein (Baldisseri and Torchia, unpublished results). However, methyl groups of a number of residues in RCAM-BPTI and BPTI have essentially the same flexibility (Richarz *et al.*, 1980), in spite of the higher melting temperature and slower amide exchange rates of the latter protein. Evidently, in SNase, the increase in thermal stability and the decrease in hydrogen exchange rates that

are caused by ligand binding are accompanied by a tightening of the internal structure of the protein in the neighbourhood of the ligand binding sites.

5 Conclusions and Perspective

We have reviewed pulsed NMR techniques for measuring A-spin relaxation, in AX and AX_3 spin systems, with high resolution and sensitivity. While we have focused upon studies of the dynamics of SNase, the backbone motions of several other ^{15}N-labelled proteins have been elucidated by use of similar techniques (Clore *et al.*, 1990b; Peng *et al.*, 1991b; Barbato *et al.*, 1992; Schneider *et al.*, 1992; Stone *et al.*, 1992; Takahashi *et al.*, 1992).

While ^{1}H-detected natural abundance ^{13}C relaxation studies are feasible at protein concentrations above 10 mM (Dellwo and Wand, 1989; Nirmala and Wagner, 1989; Palmer *et al.*, 1991a), solubility limitations will typically require enrichment levels of at least 15% to achieve the sensitivity required to measure relaxation parameters accurately. The approach taken herein, that of incorporating specific types of enriched amino acids into a protein, maximizes sensitivity and minimizes spectral overlap, but requires chemical synthesis of amino acids and multiple protein sample preparations, although the latter can be limited by incorporating several different types of amino acids into the protein.

It would be ideal if uniformly 98% ^{13}C-enriched protein samples could be used in ^{13}C relaxation studies, because such samples would yield the greatest sensitivity and, in any case, are needed to obtain side-chain carbon sequential assignments. The challenge to be overcome is the design of pulse sequences that can eliminate the effects of carbon–carbon couplings upon the relaxation measurements. In the event that this cannot be done, a sample that is 15–20% ^{13}C-enriched should provide satisfactory sensitivity and at the same time reduce the effect of homonuclear coupling to an acceptable level.

One anticipates that ^{13}C relaxation studies will provide a wealth of information about protein dynamics at a myriad of assigned sites throughout the protein, ranging from highly constrained backbone and side-chain atoms in the interior to flexible side-chain atoms near and at the protein surface. Of particular interest will be the information obtained about dynamics of protein surfaces involved in catalysis and in intermolecular interactions. Of course, in order to obtain such information one must measure thousands of signal intensities and then derive the relaxation parameters from these measurements. Newly developed processing software (Delaglio and Bax, private communication) greatly accelerates this task.

Interpreting the relaxation parameters will represent a final challenge. Although one will be able to obtain models of internal motion that are consistent with the values of S^2 and τ_e derived from the model-free analysis, a more fundamental approach would be to calculate spectral density functions and the associated relaxation parameters from molecular dynamics trajectories and compare these with the experimental results. Agreement between theory and experiment would establish the veracity of the potential functions used in the calculations, and confirm that the calculated trajectories are an accurate description of the internal motions of the protein. It seems reasonable to expect that advances in technology will make such calculations practical in the next few years.

References

Abragam, A. (1961). In Marshall, W. C. and Wilkinson, D. H. (Eds), *The Principles of Nuclear Magnetism*. Clarendon Press, Oxford, pp. 289–305

Baldisseri, D. M., Torchia, D. A., Poole, L. B. and Gerlt, J. A. (1991). Deletion of the Ω-loop in the active site of staphylococcal nuclease. 2. Effects on protein structure and dynamics. *Biochemistry*, **30**, 3628–3633

Barbato, G., Ikura, M., Kay, L. E., Pastor, R. W. and Bax, A. (1992). Backbone dynamics of calmodulin studied by ^{15}N relaxation using inverse detected two-dimensional NMR spectroscopy: the central helix is flexible. *Biochemistry*, **31**, 5269–5278

Bax, A., Clore, G. M. and Gronenborn, A. M. (1990a). ^{1}H–^{1}H correlation via isotropic mixing of ^{13}C magnetization, a new three-dimensional approach for assigning ^{1}H and ^{13}C spectra of ^{13}C-enriched proteins. *J. Magn. Reson.*, **88**, 425–431

Bloembergen, N., Purcell, E. M. and Pound, R. V. (1948). Relaxation effects in nuclear magnetic resonance absorption. *Phys. Rev.*, **73**, 679–712

Boyd, J., Hommel, U. and Campbell, I. D. (1990). Influence of cross-correlation between dipolar and anisotropic chemical shift relaxation mechanisms upon longitudinal relaxation rates of ^{15}N in macromolecules. *Chem. Phys. Lett.*, **175**, 477–482

Clore, G. M., Bax, A., Driscoll, P. C., Wingfield, P. T. and Gronenborn, A. M. (1990a). Assignment of the side-chain ^{1}H and ^{13}C resonances of interleukin-1β using double- and triple-resonance heteronuclear three-dimensional NMR spectroscopy. *Biochemistry*, **29**, 8172–8184

Clore, G. M. and Gronenborn, A. M. (1989). Determination of three dimensional structures of proteins and nucleic acids in solution by NMR spectroscopy. *CRC Crit. Rev. Biochem. Mol. Biol.*, **24**, 479–564

Clore, G. M., Kay, L. E., Bax, A. and Gronenborn, A. M. (1991a). Four-dimensional $^{13}C/^{13}C$-edited nuclear overhauser enhancement spectroscopy of a protein in solution: Application to interleukin-1β. *Biochemistry*, **30**, 12–18

Clore, G. M., Szabo, A., Bax, A., Kay, L. E., Driscoll, P. C. and Gronenborn, A. M. (1990b). Deviation from the simple two-parameter model-free approach to the interpretation of nitrogen-15 nuclear magnetic relaxation of proteins. *J. Am. Chem. Soc.*, **112**, 4989–4991

Clore, G. M., Wingfield, P. T. and Gronenborn, A. M. (1991b). High resolution three-dimensional structure of interleukin-1β in solution by three- and four-dimensional nuclear magnetic resonance spectroscopy. *Biochemistry*, **30**, 2315–2330

Cole, H. B. R. and Torchia, D. A. (1991). An NMR study of the backbone dynamics of staphylococcal nuclease in the crystalline state. *Chem. Phys.*, **158**, 271–281

Dellwo, M. J. and Wand, A. J. (1989). Model-independent and model-dependent analysis of the global and internal dynamics of cyclosporin A. *J. Am. Chem. Soc.*, **111**, 4571–4578

Ernst, R. R. (1966). Nuclear magnetic double resonance with an incoherent radio-frequency field. *J. Chem. Phys.*, **45**, 3845–3854

Fesik, S. W., Eaton, H. L., Olejneczak, E. T., Zuiderweg, E. R. P., McIntosh, L. P. and Dahlquist, F. W. (1990). 2D and 3D NMR spectroscopy employing ^{13}C–^{13}C magnetization transfer by isotropic mixing. Spin system identification in large proteins. *J. Am. Chem. Soc.*, **112**, 886–888

Goldman, M. (1984). Interference effects in the relaxation of a pair of unlike spin-1/2 nuclei. *J. Magn. Reson.*, **60**, 437–452

Haeberlen, U. (1976). High resolution NMR in solids: Selective averaging. *Adv. Magn. Reson., Suppl. 1*, 1–190

Hynes, T. R. and Fox, R. O. (1991). The crystal structure of staphylococcal nuclease refined at 1.7 Å resolution. *Protein Struct. Func.*, **10**, 92–105

Ikura, M., Kay, L. E. and Bax, A. (1990). A novel approach for sequential assignment of ^{1}H, ^{13}C, and ^{15}N spectra of larger proteins: Heteronuclear triple-resonance three-dimensional NMR spectrosocopy. Application to calmodulin. *Biochemistry*, **29**, 4659–4667

Ikura, M., Spera, S., Barbato, G., Kay, L. E., Krinks, M. and Bax, A. (1991). Secondary structure and side-chain ^{1}H and ^{13}C resonance assignments of calmodulin in solution by heteronuclear multidimensional NMR spectroscopy. *Biochemistry*, **30**, 9216–9228

Kamath, U. and Shriver, G. W. (1989). Characterization of thermotropic state changes in myosin subfragment-1 and heavy meromyosin by UV difference spectroscopy. *J. Biol. Chem.*, **264**, 5586–5592

Karplus, M. and McCammon, J. A. (1986). The dynamics of proteins. *Sci. Am.*, **254**, April, 42–51

Kay, L. E., Bull, T. E., Nicholson, L. K., Griesinger, C., Schwalbe, H., Bax, A. and Torchia, D. A. (1992a). On the measurement of heteronuclear transverse relaxation times in AX_3 spin systems via polarization transfer techniques. *J. Magn. Reson.*, **100**, 538–558

Kay, L. E., Clore, G. M., Bax, A. and Gronenborn, A. M. (1990a). Four-dimensional heteronuclear triple-resonance NMR spectroscopy of interleukin-1β in solution. *Science*, **249**, 411–414

Kay, L. E., Ikura, M. and Bax, A. (1990b). Proton–proton correlation via carbon–carbon couplings: A three dimensional NMR approach for the assignment of aliphatic resonances in proteins labeled with carbon-13. *J. Am. Chem. Soc.*, **112**, 888–889

Kay, L. E., Nicholson, L. K., Delaglio, F., Bax, A. and Torchia, D. A. (1992b). Pulse sequences for removal of the effects of cross correlation between dipolar and chemical-shift anisotropy relaxation mechanisms on the measurement of heteronuclear T_1 and T_2 values in proteins. *J. Magn. Reson.*, **97**, 359–375

Kay, L. E. and Torchia, D. A. (1991). The effects of dipolar cross correlation on ^{13}C methyl-carbon T_1, T_2 and NOE measurements in macromolecules. *J. Magn. Reson.*, **95**, 536–547

Kay, L. E., Torchia, D. A. and Bax, A. (1989). Backbone dynamics of proteins as studied by ^{15}N inverse detected heteronuclear NMR spectroscopy: Application to staphylococcal nuclease. *Biochemistry*, **28**, 8972–8979

Lipari, G. and Szabo, A. (1982a). Model-free approach to the interpretation of nuclear magnetic resonance relaxation in macromolecules. 1. Theory and range of validity. *J. Am. Chem. Soc.*, **104**, 4546–4559

Lipari, G. and Szabo, A. (1982b). Model-free approach to the interpretation of nuclear magnetic resonance relaxation in macromolecules. 2. Analysis of experimental results. *J. Am. Chem. Soc.*, **104**, 4559–4570

Loll, P. J. and Lattman, E. E. (1989). The crystal structure of the ternary complex of staphylococcal nuclease, Ca^{2+}, and the inhibitor pdTp, refined at 1.65 Å. *Proteins: Struct. Func. Genet.*, **5**, 183–201

London, R. E. (1989). Interpreting protein dynamics with NMR relaxation experiments. *Meth. Enzymol.*, **176**, 358–375

Messerle, B. A., Weder, G., Otting, G., Weber, C. and Wüthrich, K. (1989). Solvent suppression using a spin lock in 2D and 3D NMR spectroscopy with H_2O solutions. *J. Magn. Reson.*, **85**, 608–613

Nicholson, L. K., Kay, L. E., Baldisseri, D. M., Arango, J., Young, P. E., Bax, A. and Torchia, D. A. (1992). Dynamics of methyl groups in proteins as studied by proton detected ^{13}C NMR spectroscopy. Application to the leucine residues of staphylococcal nuclease. *Biochemistry*, **31**, 5253–5263

Nirmala, N. R. and Wagner, G. (1989). Measurement of ^{13}C spin–spin relaxation times by two-dimensional heteronuclear ^{1}H–^{13}C correlation spectroscopy. *J. Magn. Reson.*, **82**, 659–661

Palmer, A. G., III, Rance, M. and Wright, P. E. (1991a). Intramolecular motions of a zinc finger DNA-binding domain from Xfin characterized by proton-detected natural abundance ^{13}C heteronuclear NMR spectroscopy. *J. Am. Chem. Soc.*, **113**, 4371–4380

Palmer, A. G., III, Skelton, N. J., Chazin, W. J., Wright, P. E. and Rance, M. (1992). Suppression of the effects of cross-correlation between dipolar and anisotropic chemical shift relaxation mechanisms in the measurement of spin–spin relaxation rates. *Mol. Phys.*, **75**, 699–711

Palmer, A. G., III, Wright, P. E. and Rance, M. (1991b). Measurement of relaxation time constants for methyl groups by proton-detected heteronuclear NMR spectroscopy. *Chem. Phys. Lett.*, **185**, 41–46

Pelton, J. G., Torchia, D. A., Meadow, N. D., Wong, C. Y. and Roseman, S. (1991). ^{1}H, ^{15}N, and ^{13}C NMR signal assignments of III^{Glc}, a signal-transducing protein of *Escherichia coli*, using three-dimensional triple-resonance techniques. *Biochemistry*, **30**, 10043–10057

Peng, J. W., Thenabal, V. and Wagner, G. (1991a). Improved accuracy of heteronuclear transverse relaxation time measurements in macromolecules. Elimination of antiphase contributions. *J. Magn. Reson.*, **95**, 421–427

Peng, J. W., Thenabal, V. and Wagner, G. (1991b). 2D heteronuclear NMR measurements of spin–lattice relaxation times on the rotating frame of X nuclei in heteronuclear HX spin systems. *J. Magn. Reson.*, **94**, 82–100

Press, W. H., Flannery, B. P., Teukolsky, S. A. and Vetterling, W. T. (1988). In *Numerical Recipes in C*. Cambridge University Press, Cambridge, pp. 317–323

Richarz, R., Nagayama, K. and Wüthrich, K. (1980). Carbon-13 nuclear magnetic resonance relaxation studies of internal mobility of the polypeptide chain in basic pancreatic trypsin inhibitor and a selectively reduced analogue. *Biochemistry*, **19**, 5189–5196

Schneider, D. M., Dellwo, M. J. and Wand, A. J. (1992). Fast internal mainchain dynamics of ubiqutin. *Biochemistry*, **31**, 3645–3652

Shortle, D. (1983). A genetic system for analysis of staphylococcal nuclease. *Gene*, **22**, 181–189

Sparks, S. W., Cole, H. B. R., Torchia, D. A. and Young, P. E. (1989). Molecular dynamics and structure of staphylococcal nuclease in the crystalline state and in solution. *Chem. Scripta*, **29A**, 31–38

Stone, M. J., Fairbrother, W. J., Palmer, A. G., III, Reizer, J., Saier, M. H., Jr., and Wright, P. E. (1992). The backbone dynamics of the *Bacillus subtilis* glucose permease IIA domain determined from ^{15}N nmr relaxation measurements. *Biochemistry*, **31**, 4394–4406

Takahashi, H., Suzuke, E., Shimada, I. and Arata, Y. (1992). Dynamical structure of the antibody combining site as studied by ^{1}H–^{15}N shift correlation NMR spectroscopy. *Biochemistry*, **31**, 2464–2468

Torchia, D. A., Sparks, S. W. and Bax, A. (1989). Staphylococcal nuclease: Sequential assignments and solution structure. *Biochemistry*, **28**, 5509–5524

Torchia, D. A. and Szabo, A. (1985). The information content of powder lineshapes in the fast motion limit. *J. Magn. Reson.*, **64**, 135–141

Venable, R. M. and Pastor, R. W. (1988). Frictional models for stochastic simulations of proteins. *Biopolymers*, **27**, 1001–1014

Wang, J., Hinck, A. P., Loh, S. N. and Markley, J. M. (1990a). Two dimensional studies of staphylococcal nuclease: Evidence for conformational heterogeneity from hydrogen-1, carbon-13, and nitrogen-15 spin system assignments of the aromatic amino acids in the nuclease H124L–thymidine 3′-5′-bisphosphate–Ca^{2+} ternary complex. *Biochemistry*, **29**, 4242–4253

Wang, J., LeMaster, D. M. and Markley, J. M. (1990b). Two-dimensional NMR studies of staphylococcal nuclease. 1. Sequence-specific assignments of hydrogen-1 signals and solution structure of the nuclease H124L–thymidine 3′-5′-bisphosphate–Ca^{2+} ternary complex. *Biochemistry*, **29**, 88–101

Werbelow, L. G. and Grant, D. M. (1977). Intramolecular dipolar relaxation in multispin systems. *Adv. Magn. Reson.*, **9**, 189

Wittebort, R. J., Rothgeb, T. M., Szabo, A. and Gurd, F. R. N. (1979). Aliphatic groups of sperm whale myoglobin: ^{13}C NMR study. *Proc. Natl Acad. Sci. USA*, **76**, 1059–1063

Woessner, D. E. (1962). Spin relaxation processes in a two-proton system undergoing anisotropic reorientation. *J. Chem. Phys.*, **36**, 1–8

Wüthrich, K. (1986). *NMR of Proteins and Nucleic Acids*. Wiley, New York